



Full paper



Switchable textile-triboelectric nanogenerators (S-TENGs) for continuous profile sensing application without environmental interferences

Shuting Liu^{a,b,1}, Hao Wang^{b,c,1}, Tianyiyi He^b, Shurong Dong^{a,**}, Chengkuo Lee^{b,*}

^a Key Laboratory of Micro-nano Electronic Devices and Smart Systems of Zhejiang Province, College of Information Science & Electronic Engineering, Zhejiang University, Hangzhou, 310027, China

^b Department of Electrical and Computer Engineering, National University of Singapore, 117583, Singapore

^c Institute of Biomedical & Health Engineering, Shenzhen Institutes of Advanced Technology (SIAT), Chinese Academy of Sciences (CAS), Shenzhen, 518035, China

ARTICLE INFO

Keywords:

Switchable TENGs
Continuous sensing profile
Without environmental interferences
Textile TENGs

ABSTRACT

Conventionally, the output amplitude of triboelectric nanogenerators (TENGs) sensors is detected as the sensing output, where the accuracy and stability are easily affected by environmental interferences such as humidity, temperature and electrostatic coupling with surrounding objects. Meanwhile, the nature of pulse mode voltage output cannot provide information to further generate a detailed profile of the varying force with time interval when users press a typical TENG working in the contact-separation mode. These two critical issues hinder the TENGs sensors to be competitive with conventionally commercialized sensors. In this study, a switchable textile-triboelectric nanogenerator (S-TENG) is proposed to address these issues. By working on a switchable mode to generate resistor-capacitor (RC) discharging voltage, i.e., enabling capacitive sensing, the capacitance of the TENGs device is not affected by environmental interferences. Moreover, a high-frequency switching approach is investigated to generate a continuous profile of time-dependent capacitance as a function of force along time, referring to the continuous sensing parameter. Therefore, S-TENGs offer the sensory information which could not be achieved by any other TENGs so far.

1. Introduction

Since firstly invented by Z. L. Wang et al. [1], triboelectric nanogenerators (TENGs) have shown superior capability on energy harvesting [2–12], besides, kinds of methods were also proposed to enhance its output characteristics [13–15]. Owing to its versatile capability, a variety of self-powered sensors were developed [16–52] for various kinds of mechanical and chemical sensing applications. For the mechanical sensing applications, diversified physical factors, such as force [34,50], tactile [51–53], pressure [24], sliding [35], contact area [25], bending and tilting angle [26,46,49], rotation [27], speed [28] and acceleration [29], etc., can be sensed by using well-designed TENG structures as long as they can mechanically drive the TENG devices. By leveraging the detection of the charge density change on the specifically modified triboelectric contact surfaces as a function of targeted chemical concentration, a few liquid [30] and gas [19,31,32,46] based TENG

chemical sensors have been reported. However, the nature of TENGs not only grants its versatility on self-powered sensors but also brings other issues. TENGs devices are always operated mechanically at environment with a set of specific parameters, such as force, speed, and frequency, where the fluctuation of temperature, humidity and electrostatic coupling from the surrounding environment also affect on the TENG output. When users emphasize on detecting one of the parameters, others are deemed to become interference parameters and such influence is difficult to be eliminated. For example, in the force sensing application, the output of the TENGs device is not only measured as a function of the applied force but also affected by other factors, such as the force speed, the contact area and humidity. Therefore, good measurement accuracy and repeatability of the output amplitude is questionable, or not achievable, if the interferences are not able to be eliminated. Another issue is insufficiency sensing information. In the non-open-circuit condition, it is well-known that the TENGs device only

* Corresponding author. E2-03-29 Electrical and Computer Engineering, National University of Singapore, 4 Engineering Drive 3, 117583, Singapore.

** Corresponding author. College of Information Science and Electronic Engineering, Zhejiang University, No.38 Zheda Road, Xihu District, Hangzhou, Zhejiang, 310027, China.

E-mail addresses: dongshurong@zju.edu.cn (S. Dong), elelc@nus.edu.sg (C. Lee).

¹ Shuting Liu and Dr Hao Wang contribute equally to this manuscript.

generates two peaks in one operation cycle. It is hard to get sufficient information to reproduce a continuous profile representing the variation of the sensing-parameter, e.g., a gradually changed force applied on a TENGs device. These two issues are the major obstacles to make TENGs sensors not able to compete with other commercialized sensors.

In this study, a switchable textile-TENGs (S-TENGs) is proposed to solve these two issues. Simply speaking, S-TENGs is a textile-based soft TENGs device with a switchable operation method to achieve self-powered capacitive sensing. The switchable operation method is firstly developed by Z. L. Wang et al. [54–56], which converts the continuous triboelectric output to a standard RC discharge by a switching operation for output amplification. In this switchable operation, an RC discharge happens when the switch is closed. With a known load impedance R , the instantaneous capacitance, C of the TENGs device can be decoded from the measured time constant $\tau = RC$, which is a capacitive sensing scenario. This instantaneous capacitance is a very reliable characterization of the mechanical status of the TENGs device, which is determined by the mechanical operation and not affected by temperature, humidity and electrostatic coupling of the surrounding environment. Therefore, the time constant τ which represents the C will be a much more stable and reliable sensing output compared with the voltage amplitude. If instead of closed twice, the switch is periodically closed during the whole operation to generate multiple RC discharging outputs, we can plot a series of τ to form a τ curve, as the characterization of a continuous and smooth capacitance variation of TENGs sensors. Based on the practical applications, this τ curve can represent the profile of the sensing factors, such as force, weight and bending, which will be demonstrated in this study.

2. Results & discussion

Since the operation method is changed, the optimization target of the S-TENGs is quite different. In the conventional TENGs devices, the total energy during the whole operation cycle is desired to be maximum. In S-TENGs, each closing of the switch depletes the energy accumulated in the TENGs device. Thus, the amplitude of each RC discharging peak is determined by the energy generated during the time interval between two switching operations, which is not related to the total energy generated in the whole operation cycle but affected by the energy density with respect to the total device volume. In other words, it is the energy density other than the total energy to be maximized for the structural design for the highest voltage amplitude.

The general working principle of the switch involved TENGs is shown in Fig. 1(a1) and its equivalent circuit is shown in Fig. 1(a2) and (a3). During the operation cycle, the switch is closed only at the stages of fully pressed, when the spacing of the device, d , reaches the minimum, d_{min} , and fully released, when d reaches the maximum, d_{max} . The closing of the switch depletes the energy accumulated in the TENGs device to induce an RC discharging and generate an exponential voltage waveform. According to the current flow direction, the polarity of the exponential voltage can be reversed as shown in Fig. 1(a4).

Fig. 1(b) and (c) illustrates the optimization of the energy density for the switch involved TENGs system. Firstly, the parasitic capacitance induced by the electrostatic coupling is considered for the expression of the energy output. The electric field induced by the electrostatic charge from triboelectrification is not all confined within the TENGs device but partially coupled into the surrounding objects shown in Fig. 1(b1). This effect can be modeled as some parasitic capacitors in Fig. 1(b2) and as C_p connected in parallel with the capacitance of the TENGs device, C_{TENG} , as shown in Fig. 1(b3). Then the energy stored in the system can be

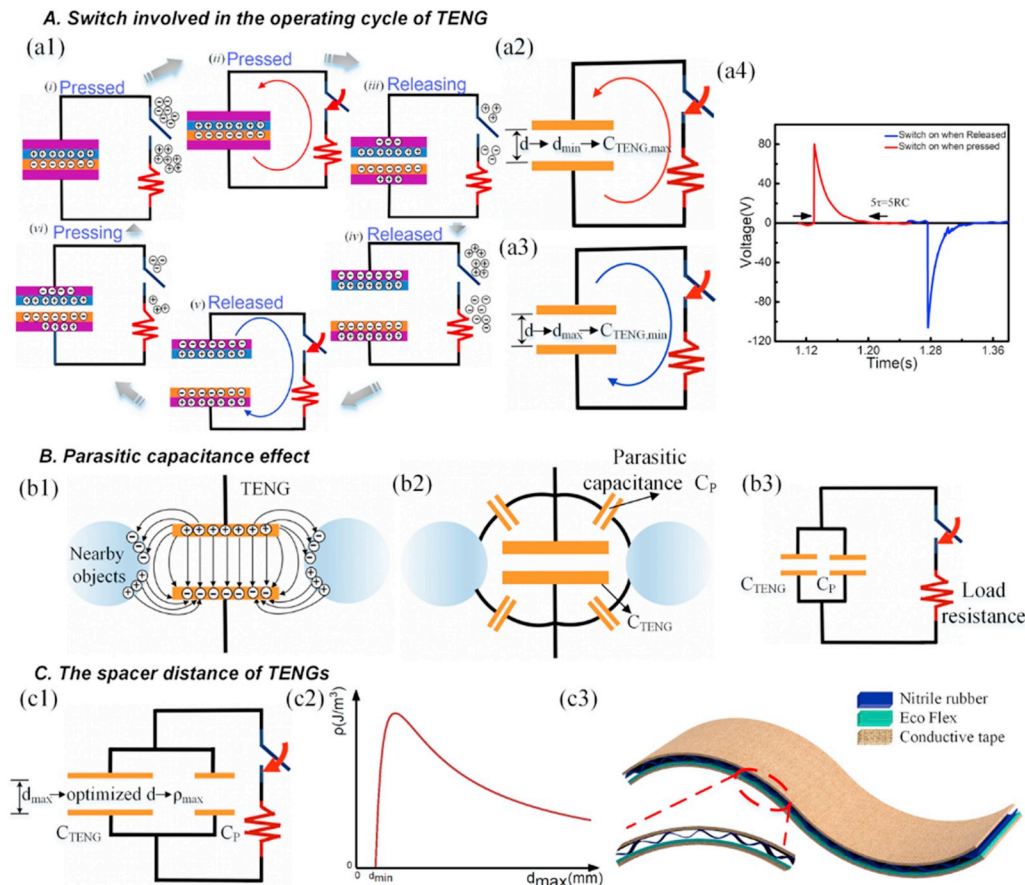


Fig. 1. The working principle of the switchable TENGs and the optimization for the energy density ρ . (a1) Circuit connection, operation cycle and working mechanism of switchable TENGs; (a2) and (a3) Equivalent circuit of the switchable TENGs; (a4) The output characteristics of switchable TENGs when the switch is closed at d_{min} and d_{max} respectively, R is 10 M Ω . (b1) The electrostatic charges of two triboelectric layers are partially coupled by nearby. (b2) and (b3) The equivalent circuit to model the effect of the parasitic capacitance. (c1) and (c2) The relationship between ρ and d_{max} . (c3) The structure of soft, textile based TENGs with optimized d_{max} .

expressed as:

$$E = \frac{1}{2} \times \frac{Q^2}{C_p + C_{TENG}} \quad (1)$$

The energy output, E_{output} , during the operation, can be considered as the energy change of the system, ΔE , expressed as:

$$\Delta E = E_{max} - E_{min} = \frac{1}{2} \times \left(\frac{Q^2}{C_p + C_{TENG_{min}}} - \frac{Q^2}{C_p + C_{TENG_{max}}} \right) \quad (2)$$

Here

$$C_{TENG} \approx \varepsilon \frac{A}{d} \quad (3)$$

Then the capacitance of the fully pressed device is

$$C_{TENG_{max}} \approx \varepsilon \frac{A}{d_{min}} \quad (4)$$

while the capacitance of the fully released device is

$$C_{TENG_{min}} \approx \varepsilon \frac{A}{d_{max}} \quad (5)$$

Where A and d refer to the area and spacing of the TENGs device, respectively. Then the energy density, ρ , of the system can be expressed as a function of d_{max} since d_{min} is a non-zero constant:

$$\rho = \frac{E_{output}}{A \times d} = \frac{1}{2} \times \frac{\frac{Q^2}{C_p + \varepsilon \frac{A}{d_{min}}} - \frac{Q^2}{C_p + \varepsilon \frac{A}{d_{max}}}}{A \times d_{max}} = f(d_{max}) \quad (6)$$

Then consider two conditions when $d_{max} = d_{min}$ and $d_{max} = \infty$:

$$f(d_{min}) = 0 \quad (7)$$

$$f(\infty) = 0 \quad (8)$$

The energy density at these two extreme conditions is zero as plotted in Fig. 1(c2), there should be an optimized d_{max} to achieve ρ_{max} . In the testing, this optimized d_{max} is a relatively small value, which will be detailed characterized in Fig. 2. Therefore, to achieve this maximum energy density, a soft textile-based TENGs device of a narrow gap is designed to fit the optimized d_{max} as shown in Fig. 1(c3). The nitrile rubber and EcoFlexTM-00-30 are utilized as positive and negative tribo-material, respectively, owing to their soft nature and large

electronegativity difference. Single side conductive Ni fabric tapes are used as electrodes for both of them. The gap distance created by the folds on the nitrile rubber generally fits the optimized value, which is measured as 0.25 mm in Fig. 2. The detailed fabrication process is shown in Fig. S1 (see Supporting information). The exact gap spacing is controlled by the amount the wrinkles as shown in Fig. S2.

To explore the optimization spacer distance d_{max} , a 5-layer zigzag TENGs, which enables a well-controlled spacing, is used for a test. The effective area is $6 \times 6 \text{ cm}^2$ and all layers are connected in parallel. For a better study of the output of releasing, a diode is added to remove the voltage output of pressing. The materials for contact surfaces are the same as the S-TENGs.

The d_{max} of TENGs equals to the height difference when the device is fully pressed and released. Then the d_{max} is controlled by the releasing height. To compare the output characteristics of TENGs with a switch (TENG-WS) and without a switch (TENG-WOS), the voltage output with different d_{max} and load resistance are measured. Fig. 2(b) shows the data samples when the load resistance is 10 M Ω . As seen, the voltage for TENG-WS is always an exponential waveform while the ones for TENG-WOS are broad peaks. The output energy is further calculated from the exact waveforms as shown in Fig. 2(b). Since the load resistance is the exclusive energy consumer in the circuit, the output energy should not change with load resistance, which is confirmed by the curve of TENG-WS. Then the energy density by changing the d_{max} is shown in Fig. 2(d). As seen, it follows the same curve in Fig. 1(c2) and the optimized value of the d_{max} for a 5-layer device is 1.2 mm. Then the d_{max} for a single layer is about 0.25 mm. Other detailed device characterization for TENG-WS and TENG-WOS can be found in Fig. S3 (Supporting Information). Then the S-TENGs is prepared based on the optimized d_{max} . Due to the soft nature of the textile materials, the device can be operated in several different modes, such as tapping, folding and wrapping as shown in Fig. 2(e). One of the advantages of the S-TENGs is that the voltage amplitude is not affected by the operation speed. For conventional TENGs, which is TENG-WOS here, the voltage amplitude will increase with contact-separation speed, which is the tapping speed. However, a textile device always follows a gradual contact-separation pattern, introducing a slow contact-separation speed. Thus, the textile-based TENGs normally cannot achieve a high voltage output. However, for the cases with a switch, which is TENG-WS, the energy can be accumulated before releasing and the tapping speed does not affect the output, as shown in Fig. 2(f-g). The similar data for the other two

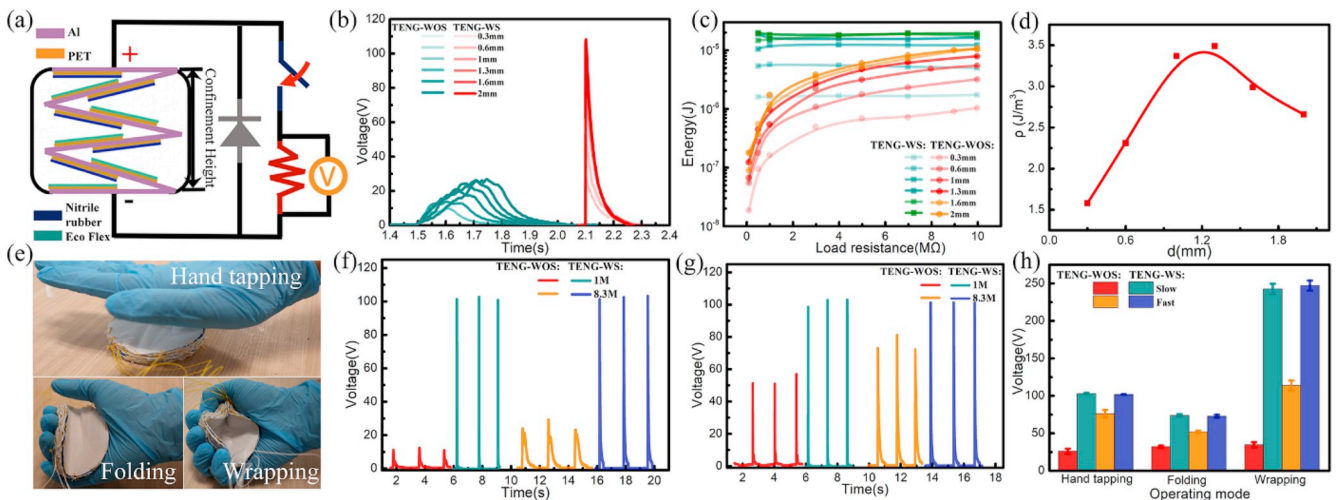


Fig. 2. The optimization of the d_{max} and the characterization of S-TENGs. (a) Testing configuration for the zigzag TENGs. (b) output voltage curves for TENG-WS and TENG-WOS with different spacer distances from 0.3 to 2 mm, respectively, R is 10 M Ω . (c) The effect of the d_{max} and load resistance on the output energy of TENG-WS and TENG-WOS. (d) The curve of energy density with respect to the d_{max} . (e) Three typical operating modes for S-TENG. (f-g) The comparison of output voltage curves between TENG-WS and TENG-WOS when the device is tapped at a low (f) and high (g) speed, respectively. (h) The comparison of voltage amplitude between TENG-WS and TENG-WOS when the device is tapped, folded and wrapped, respectively. R is 8.3 M Ω .

operation modes, folding and wrapping can be found in Fig. S4 (Supporting Information). Fig. 2(h) summarizes the voltage amplitude with different operation speed for TENG-WS and TENG-WOS in three operation modes.

As demonstrated above, the time constant, $\tau = RC$, refers to how the device is squeezed either by force of bending. Then any interference factors, which do not affect the capacitance of the device, can be eliminated by the measurement of τ . The capacitance is calculated from equation (3), and the humidity has no effect on both the area, A , and the spacing, d , and only has a slight effect on the permittivity, ϵ . Thus, the effect of humidity can be eliminated. Therefore, a new sensing mechanism by measuring the time constant, τ , is proposed for stable and reliable TENGs sensors. Here two general and fundamental sensing scenarios, static sensing and dynamic sensing, are demonstrated. In the future, various sensing applications can be developed based on these two scenarios.

One of the direct applications of the static scenario of S-TENGs is a self-powered weight scale as shown in Fig. 3. The weight of the object on the device can be directly measured from the time constant of the exponential output voltage waveform. The circuit and testing configuration are shown in Fig. 3(a) and Fig. S5 (Supporting Information). A tray is put on the device for a uniform weight distribution from the object. The voltage waveform on a fixed resistance, which is 8.3 M Ω , is measured. Since only the waveform of pressing is required in this application, a diode is connected to remove the interference of the releasing signal. The operation of the measurement is simple, which can be found in Video S1 (Supporting Information). An object is put on the tray then switch is pressed to generate an exponential voltage waveform. Then the exact weight is measured by calibrating τ . Since this is a manual operation, the time interval from putting the object to pressing the switch will affect the amplitude of the output voltage because of the energy accumulated in the device will have a dissipation with time. Fig. 3(b–c) shows the effect of this time interval on the voltage amplitude and the time constant. The time points for calculating τ , where amplitude decrease to $1/e$ of its peak value, are labeled as red points. As seen in Fig. 3(b), the amplitude decreases with this time interval while the τ almost keeps the same. Fig. 3(c) summarizes this trend in Fig. 3(b). Fig. 3(d–f) shows the effect of the weight and humidity on the voltage

amplitude and time constant. The τ increases with weight (Fig. 3(d)) but is not affected by the humidity (Fig. 3(e)). However, the amplitude is highly affected by the humidity. The summarized calibration by changing the humidity and weight is shown in Fig. 3(f). The two curves of the measured τ under different humidity levels almost have no difference. However, for the curves of measured voltage, a 10% RH increment causes about 80% voltage drop. This test clearly demonstrates that the measurement of the τ can effectively remove the interference of humidity in sensing applications. It is noticed that the whole τ curve is not linear. It will be more linear and sensitive at small force range. Thus, a very detailed calibration from 0–2 N is shown in Fig. 4(a). The sensing accuracy is 0.2 ms/N.

Supplementary video related to this article can be found at <https://doi.org/10.1016/j.nanoen.2020.104462>.

A natural extension of this scenario is that: if the force applied is not static but dynamically changing, can this device generate a force profile, which is highly desired for quite a lot of actual sensing applications? In operation of S-TENGs, the criterion for a voltage generation when you close the switch is that there should have a certain force variation. Then close the switch when the force is changed, the changing profile of the force can be sensed.

A simple demonstration is shown in Fig. 4. The actual operation can be found in Video S2 (Supporting Information). Five 45-g weights are put on the tray one by one then removed one by one. The switch is closed for each change of the number of weights to generate a series of voltage peaks as shown in Fig. 4(b). It is emphasized that the diode in Fig. 3(a) is removed since now we need to sense both the pressing and releasing procedures. As seen, the peaks are positive for weight increasing and negative for weight decreasing, meaning the polarity can show the changing trend of the force. Then the measured τ of each signal generally shows the force profile. It is noticed that the maximum τ does not happen at the maximum weight but has one signal delay, which is the signal after the maximum weight. Meanwhile, the end of the curve does not recover to its initial value. This is because of the response time of textile materials. It takes some time for the textile to reach the equilibrium deformation when an external force is applied, which can be considered as a response delay. This indicates that the device should be further optimized to overcome this issue. Considering that the soft

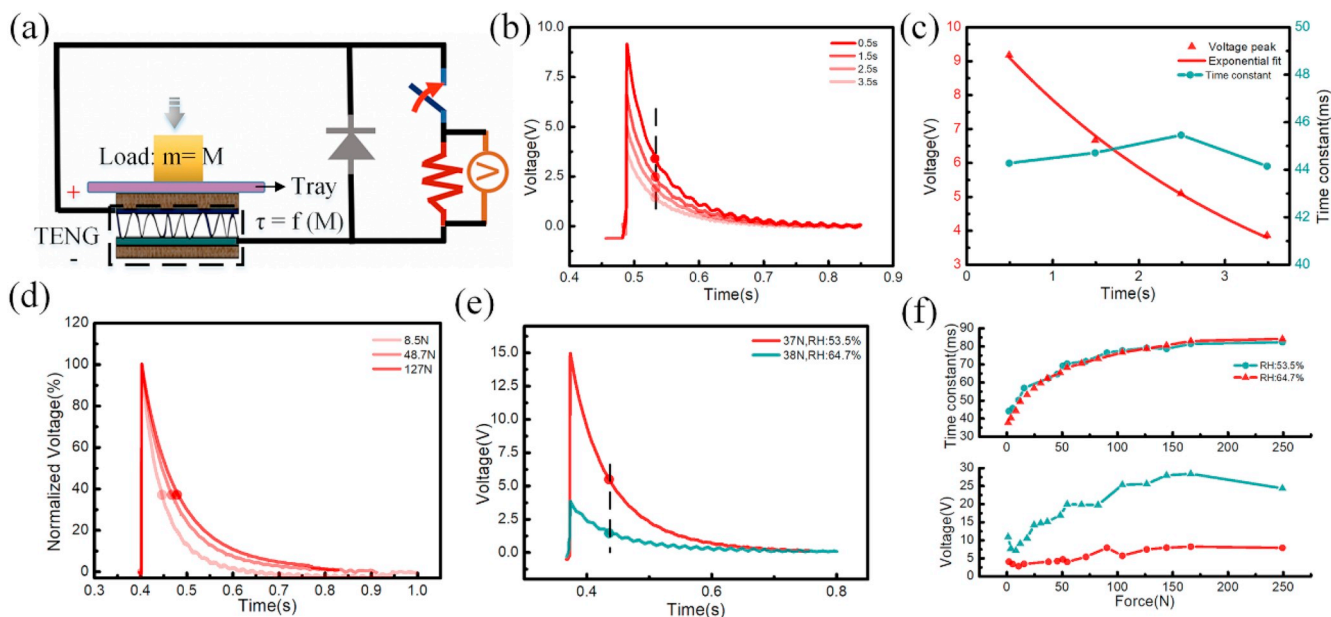


Fig. 3. Demonstration of static sensing scenario. (a) Testing configuration of weight scale; (b) The RC discharging voltage waveforms with different time interval from putting the object to pressing the switch; (c) The amplitude and τ of the waveforms in (b); (d) The normalized voltage waveforms with different weight put on the tray; (e) The voltage waveforms with the same weight in different RH levels; (f) The characterization of the weight- τ curve and weight-voltage peak curve with different RH levels.

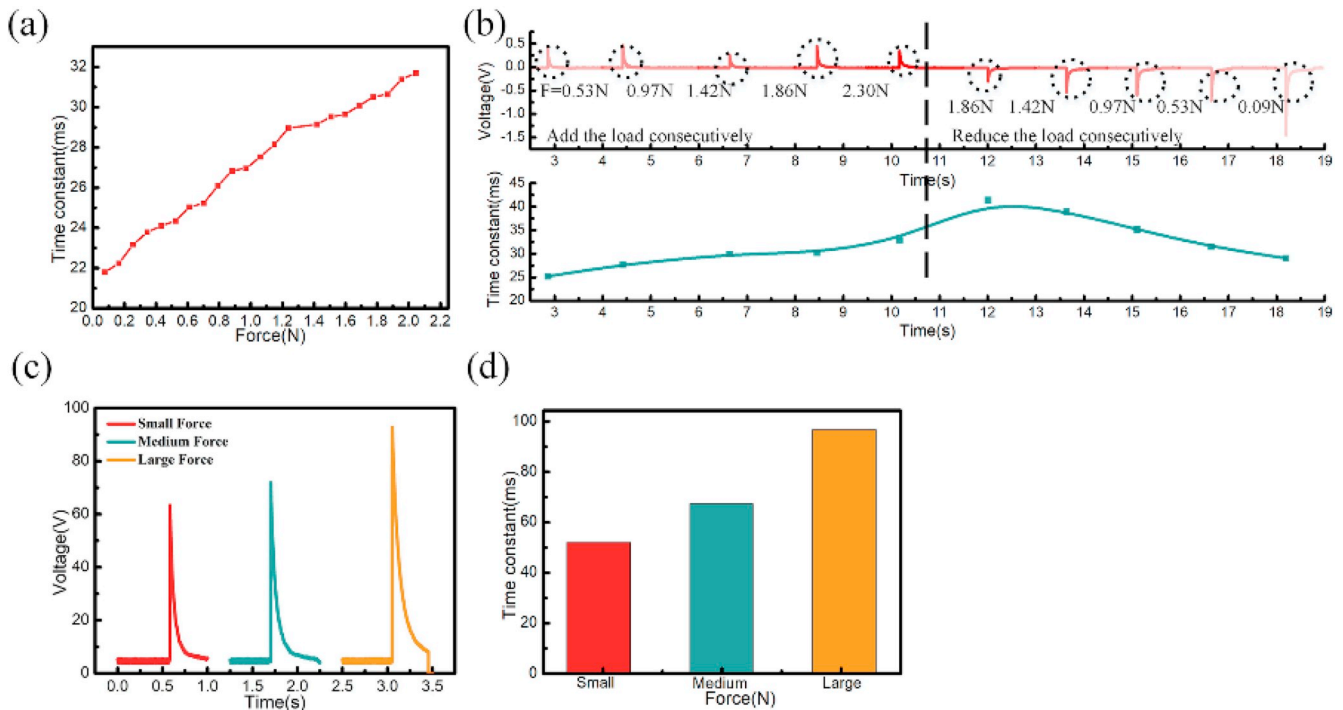


Fig. 4. Demonstration of the static sensing applications. (a) A detailed characterization of the weight- τ curve at a small force range from 0–2 N; (b) Demonstration of continuous weight sensing; (c–d) The characterization of S-TENGs when it is used to measure the hand grip strength: (c) output voltage curves under different the hand grip strength. (d) The calculated time constant from (c).

device can also be folded rather than be pressed, it can also be used to measure the hand gripping strength when the device is folded by hands, as shown in Fig. 4(c–d). Since the hand gripping force is not unidirectional, it is difficult to directly measure the applied force. Thus, we only roughly use small, medium and large force to characterize the result.

Supplementary video related to this article can be found at <https://doi.org/10.1016/j.nanoen.2020.104462>.

In the application of sensing a dynamically changing force, we can boost up the tapping frequency of the switch, named as switching frequency f_s , to acquire a smoother force profile. A comprehensive explanation for the data analysis is illustrated in Fig. 5(a). There are three data dimensions for us to decode the force. The first dimension is from the polarity of the output, which is determined by the operation trend. According to the exact application, it is defined that the pressing or bending the device generates positive peaks while releasing or stretching the device generates negative peaks. Secondly, the exact amplitude of the peaks refers to the derivative of force with respect to time, dF/dt . Since the voltage amplitude refers to the energy generated during the time interval between two switching operations, $\Delta t \approx 1/f_s$, then the voltage peak, V_p , can be considered as a function of generated energy, E . Meanwhile, the generated energy is proportional to the force change during Δt , then V_p is a function of dF/dt , shown as below when f_s is a constant.

Therefore, a curve of dF/dt can be plotted from the acquired data. Thirdly, for each peak, the τ can be calculated as the sensing result of the exact force at the time point when the switch is closed. A curve of force with respect to time can be plotted. Moreover, since τ is proportional to F , $d\tau/dt$ also refers to dF/dt . Theoretically, the two curves of $d\tau/dt$ and V_p will match with each other. Therefore, in the data analysis, there are four curves to be presented: the original measured voltage waveforms, the curve of the peak values V_p , the curve of decoded time constant τ and the curve of $d\tau/dt$.

Here two different applications are demonstrated for this dynamic sensing. One is to sense the bending angle of the elbow by attaching the device on the inner side of the cloth. Another is to sense the stepping

force of foot by attaching the device inside a shoe at the heel position. The detailed demonstration video can be found in Videos S3 and S4 (Supporting Information). The circuit used in dynamic sensing shown in Fig. 5(b) is a bit different from the one used in static sensing: the diode is removed.

Supplementary video related to this article can be found at <https://doi.org/10.1016/j.nanoen.2020.104462>.

Fig. 5(c–d) and (f–h) shows the angle sensing of the elbow. Firstly, a detailed τ - θ curve in Fig. 5(c) showing the relationship between the bending angle, θ , of the elbow and the measured τ . The red and green dots refer to the data measured from stretching and bending the arm, respectively, showing a negligible hysteresis. The sensing accuracy is 0.0044 ms/degree. Then a dynamic sensing procedure by continuously bending and stretching the arm between 0° and 90° was performed at different f_s , ranging from 2 Hz to 4 Hz by hand tapping, shown in Fig. 5(f–h). All (i) figures show the raw data from the recording. Then the exact τ of each peak is calculated to plot the curve shown in all (ii) figures. With the calibration curve in Fig. 5(c), a θ curve can be further decoded. Based on the τ curves, the derivative curves of $d\tau/dt$ are plotted as yellow curves in all (iii) figures. As a comparison, the curves of the voltage peak, V_p , are also plotted as blue curves. This V_p curve represents the derivative of the bending angle, $d\theta/dt$. As seen, the curves of $d\tau/dt$ and V_p match with each other, validating the theory. Meanwhile, a higher f_s can achieve a higher sensing resolution and generate a smoother profile of the sensing angle.

Fig. 5(h–k) shows the force sensing of the foot stepping. The data is recorded and analyzed in the same way. Since the detailed τ - F curve has been calibrated in Fig. 4(a), the calibration is not repeated here. The foot stepping upon the device is repeated with f_s from 2 Hz to 4 Hz. It is the same as in the elbow sensing, a higher f_s can achieve a higher sensing resolution. It is noticed that the stepping force was kept for a while in the testing. This kept force can be reproduced in the sensing results when the f_s is 4 Hz. Also as confirmed in its (iii) figure, in the duration of force keeping, the value of the derivative is zero.

Apparently, to achieve a better sensing resolution, a higher f_s is

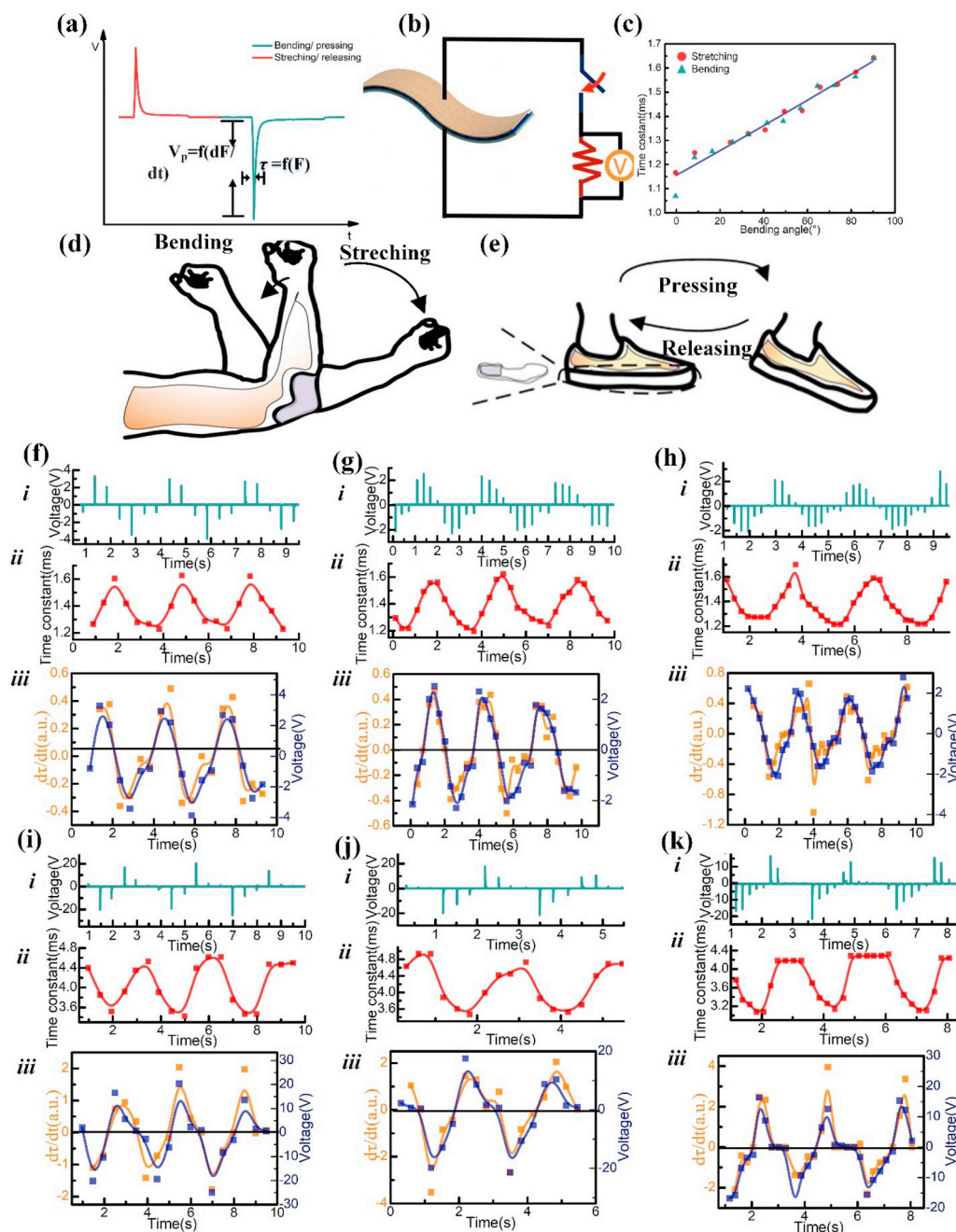


Fig. 5. Demonstration of dynamic sensing. (a) The method to analyze the measured data: The polarity represents the working condition of the device, positive peaks refer to stretching in angle sensor and releasing in force sensor; negative peaks refer to bending angle sensor and pressing in force sensor; the τ represents the sensing output; the voltage amplitude represents the derivative of the sensing output, which is dF/dt in force sensor and $d\theta/dt$ in angle sensor; (b) The testing configuration of the angle sensor and force sensor; (c) The characterization of the relationship between bending angle and the τ ; (d) The scenarios of bending angle sensor when the device is attached to the elbow; (e) The scenarios of force sensor when the device is put in the shoe; (f–h) The sensing results with different tapping frequency: (e) 2 Hz; (f) 3 Hz; (g) 4 Hz; all (i) refer to the raw data of the measured voltage curves; all (ii) refer to the decoded τ curves; all (iii) refer to the $d\tau/dt$ curves and voltage peak V_p curves; (i–k) The sensing results with different tapping frequency: (i) 2 Hz; (j) 3 Hz; (k) 4 Hz; all (i) refer to the raw data of the measured voltage curves; all (ii) refer to the decoded τ curves; all (iii) refer to the $d\tau/dt$ curves and voltage peak V_p curves.

preferred but is out of the capability of handing tapping. A simple alternative approach is to replace the mechanical switch with a MOSFET. The on/off of the MOSFET can be controlled by a clock signal. The detailed circuit and test configuration are shown in Fig. 6(a). A demonstration of sensing the tapping force is shown in Fig. 6(b–d) with f_s from 20 Hz to 80 Hz. The on-duration of the clock signal for each cycle is always 5 ms. As seen, for the f_s of 20 Hz, the force sensing curve is quite smooth. This continuous and smooth force sensing curve cannot be achieved by conventional TENGs sensors but now can be easily achieved by S-TENGs with a high f_s recording system. The detailed demonstration video can be found in Video S5 (Supporting Information).

Supplementary video related to this article can be found at <https://doi.org/10.1016/j.nanoen.2020.104462>.

However, for a higher f_s , which are the cases of 40 Hz and 80 Hz, the resolution of the sensing curves seems to have deterioration. This is a noticeable issue for high f_s recording. As seen from Fig. 6(b–d), a high f_s

provides a higher resolution but also reduces the amplitude of each peak, which is from 20 V for 20 Hz to 5 V for 80 Hz. The total energy in one operation cycle is conserved and consumed by all peaks, a higher f_s will reduce the energy for each peak, thus reduce the amplitude. Since the τ is decoded from the exact waveform of each peak, the noise will attenuate the waveform and further deteriorate the accuracy of τ . A lower voltage amplitude makes the accuracy of the decoded τ more vulnerable to the attenuation by the noise. Therefore, here is a trade-off between resolution and accuracy. A system with higher energy to increase the amplitude of each peak can enhance the accuracy of decoded τ and also boost up the f_s . In future work, a material optimization to increase the energy output is critical for the performance improvement of the device.

Meanwhile, there are always some data points, whose amplitude are very low, generating unreliable τ even if the f_s is low. Thus, an algorithm is developed to find and correct these error data points with the

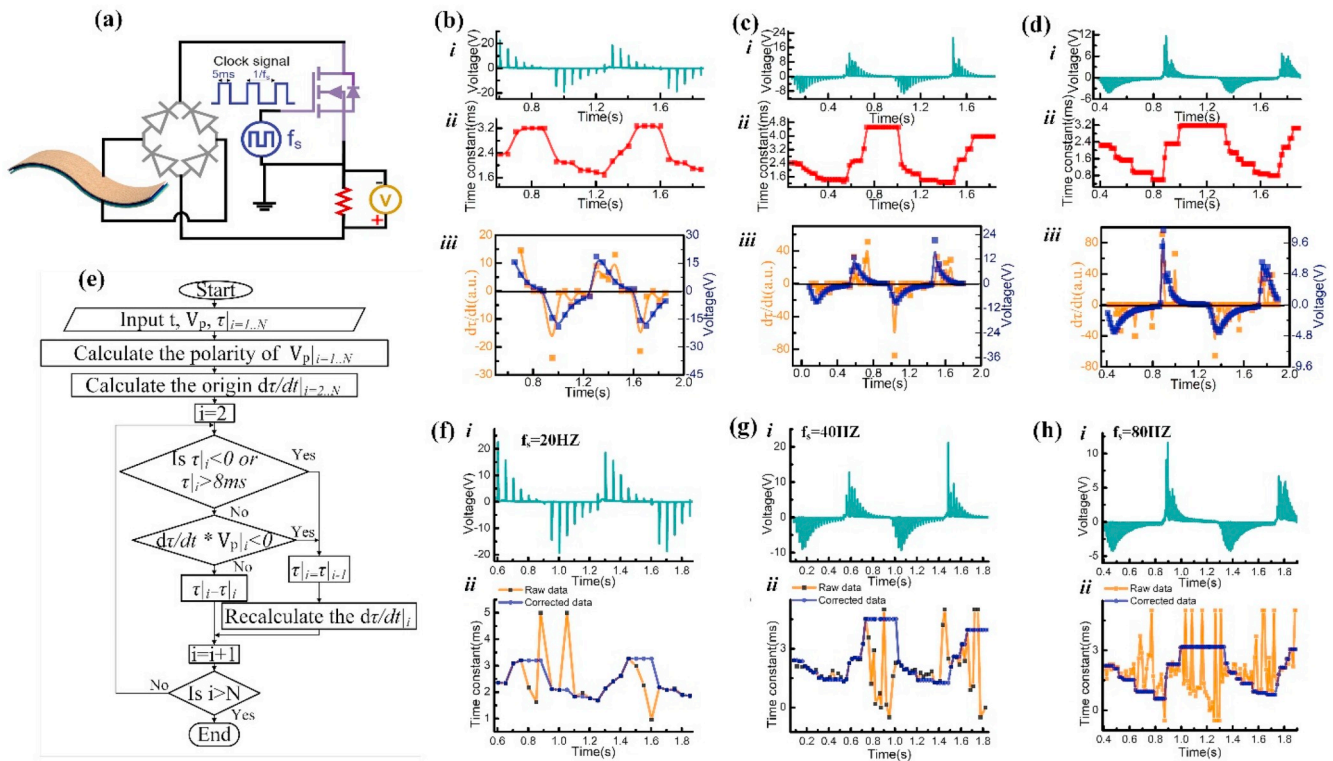


Fig. 6. The testing circuit configuration by using a MOSFET as a switch and the algorithm to correct the error data and the comparison of the data before and after the correction. (a) The testing circuit configuration by using a MOSFET as a switch; (b–d) The sensing results with different f_s : (m) 20 Hz; (n) 40 Hz; (o) 80 Hz. (e) The detailed flow chart of the algorithm; (f–h) The data comparison before and after the correction: all (i) refer to the measured voltage curves with f_s of (b) 20 Hz; (c) 40 Hz; (d) 80 Hz; all (ii) refers to the τ curve before and after the correction.

information of $d\tau/dt$ and V_p . The flow chart is shown in Fig. 6(e) and its principle is explained below.

As mentioned above, the changing trend of curves of $d\tau/dt$ and V_p should match with each other. Here the $d\tau/dt$ calculated from the τ curve is also vulnerable to the noise. However, the noise only attenuates the shape of the waveform but cannot alter the polarity. So the polarity is a stable indicator of the changing trend of the sensing parameter, which is represented by $d\tau/dt$. Therefore, the diagnosis of error data is based on the polarity mismatch between $d\tau/dt$ and V_p . Since these error data always happens when the force tends to get stabilized, an approximation is applied that the force change for error data can be neglected. Then the error data gets the same τ as the one before it. This correction results in the flat curves shown in Fig. 6(b–d). As seen, these flat curves tend to happen when the force reaches a maximum or minimum. A comparison of the decoded τ curves from 20 Hz to 80 Hz before and after the correction are shown in Fig. 6(f–h). As seen, for the case of 20 Hz, since the amplitude is higher, only a few points need correction. But for the case of 80 Hz, much more data points need to be corrected due to the lower voltage amplitude. The detailed algorithm can be found in the Supporting information S6.

Since in this study, the S-TENGs is more like a sensing approach rather than an exact device, we prepared a detailed comparison with other types of sensing mechanisms and approaches in the Supporting information S7.

3. Conclusions

In conclusion, a switchable textile-triboelectric nanogenerator (S-TENG) is proposed to achieve a self-powered capacitive sensing. Instead of measuring the voltage amplitude, which is common for conventional TENGs sensors, the time constant τ , referring to the instantaneous capacitance of the device, is decoded as the sensing output. This self-powered capacitive sensing offers quite a lot of exclusive advantages.

Firstly, it can eliminate all environmental interferences, such as temperature and humidity, to make the sensing output stable and reliable. Secondly, it can be used for the sensing of a static force value or a dynamic force profile. For the dynamic force profile, the resolution can be enhanced by boosting up the switching frequency, which can be easily achieved by a MOSFET. Lastly, instead of measuring the amplitude only, there are three data dimensions available in our approach: the voltage amplitude, V_p , the decoded time constant, τ , and the derivative of the time constant, $d\tau/dt$. These three data dimensions not only allow us to generate the sensing output but also enable a data correction to further improve the sensing accuracy.

4. Materials and methods

4.1. Preparation of the device

The preparation of EcoFlex™ 00–30: First, the mixture of Parts A and B (EcoFlex™ 00–30) with either volume or weight ratio of 1:1 was dispersed thoroughly for about 3 min, then the blend was uniformly coated on Ni electrode and baked with 70 °C in the oven for about 30 min.

4.2. Characterization of the S-TENG

The output voltage and was measured by DSOX3034A oscilloscope (Agilent).

Author contributions

The manuscript was written through contributions of all authors. The concept is proposed by Hao Wang and the experiments were performed by both Hao Wang and Shuting Liu. All authors have given approval to the final version of the manuscript. ¹These authors contributed equally.

Declaration of competing interest

The authors declare that they have no known competing financial interests or personal relationships that could have appeared to influence the work reported in this paper.

Acknowledgements

Shuting Liu appreciated the scholarship support for her visiting PhD student at NUS by the grant from National Key R&D Program of China (2018YFB2002500). S. Liu and S. Dong thank the financial support from National Natural Science Foundation of China (No. 61875015, 31571006), Zhejiang Lab (No.2018EB0ZX01), Zhejiang Province Key R&D programs (2018C01037). This work has been conducted at NUS and is supported by the grants from the National Research Foundation Competitive research programme (NRF-CRP) 'Energy Harvesting Solutions for Biosensors' (R-263-000-A27-281), National Research Foundation Competitive research programme (NRF-CRP) 'Piezoelectric Photonics Using CMOS Compatible AlN Technology for Enabling The Next Generation Photonics ICs and Nanosensors' (R-263-000-C24-281), Faculty Research Committee (FRC) 'Thermoelectric Power Generator (TEG) Based Self-Powered ECG Plaster - System Integration (Part 3)' (R-263-000-B56-112), HIFES Seed Funding 'Hybrid Integration of Flexible Power Source and Pressure Sensors' (R-263-501-012-133) and Shenzhen Science and Technology Research Program (JCYJ20170818154035069). Interests of intelligent property should refer to NUS.

Appendix A. Supplementary data

Supplementary data to this article can be found online at <https://doi.org/10.1016/j.nanoen.2020.104462>.

References

- [1] F.-R. Fan, Z.-Q. Tian, Z.L. Wang, *Nano Energy* 1 (2012) 328–334.
- [2] H. Ouyang, J. Tian, G. Sun, Y. Zou, Z. Liu, H. Li, L. Zhao, B. Shi, Y. Fan, Y. Fan, Z. L. Wang, Z. Li, *Adv. Mater.* 29 (2017) 1703456.
- [3] S. Cheon, H. Kang, H. Kim, Y. Son, J.Y. Lee, H.-J. Shin, S.-W. Kim, J.H. Cho, *Adv. Funct. Mater.* 28 (2018) 1703778.
- [4] X. Chen, Y. Wu, A. Yu, L. Xu, L. Zheng, Y. Liu, H. Li, Z. Lin Wang, *Nano Energy* 38 (2017) 91–100.
- [5] X. Cao, Y. Jie, N. Wang, Z.L. Wang, *Adv. Energy Mater.* 6 (2016) 1600665.
- [6] Y. Jie, X. Jia, J. Zou, Y. Chen, N. Wang, Z.L. Wang, X. Cao, *Adv. Energy Mater.* 8 (2018) 1703133.
- [7] Y. Jie, Q. Jiang, Y. Zhang, N. Wang, X. Cao, *Nano Energy* 27 (2016) 554–560.
- [8] X. Chen, J. Xiong, K. Parida, M. Guo, C. Wang, C. Wang, X. Li, J. Shao, P.S. Lee, *Nano Energy* 64 (2019) 103904.
- [9] W. Zhong, L. Xu, H. Wang, D. Li, Z.L. Wang, *Nano Energy* 66 (2019) 104108.
- [10] L. Liu, Q. Shi, J.S. Ho, C. Lee, *Nano Energy* 66 (2019) 104167.
- [11] J. Wang, T. He, C. Lee, *Nano Energy* (2019) 104039.
- [12] C. Yang, G. Yang, Q. Ouyang, S. Kuang, P. Song, G. Xu, D.P. Poenar, G. Zhu, K.-T. Yong, Z.L. Wang, *Nano Energy* 64 (2019) 103901.
- [13] X. Ma, S. Li, S. Dong, J. Nie, M. Iwamoto, S. Lin, L. Zheng, X. Chen, *Nano Energy* 66 (2019) 104090.
- [14] M. Khorsand, J. Tavakoli, K. Kamanya, Y. Tang, *Nano Energy* 66 (2019) 104115.
- [15] L. Shi, S. Dong, H. Xu, S. Huang, Q. Ye, S. Liu, T. Wu, J. Chen, S. Zhang, S. Li, X. Wang, H. Jin, J.M. Kim, J. Luo, *Nano Energy* 64 (2019) 103960.
- [16] L. Dhakar, S. Gudla, X. Shan, Z. Wang, F.E. Tay, C.H. Heng, C. Lee, *Sci. Rep.* 6 (2016) 22253.
- [17] Q. Shi, H. Wu, H. Wang, H. Wu, C. Lee, *Adv. Energy Mater.* 7 (2017) 1701300.
- [18] Q. Shi, H. Wang, T. Wang, C. Lee, *Nano Energy* 30 (2016) 450–459.
- [19] H. Wang, H. Wu, D. Hasan, T. He, Q. Shi, C. Lee, *ACS Nano* 11 (2017) 10337–10346.
- [20] Z. Liu, Y. Ma, H. Ouyang, B. Shi, N. Li, D. Jiang, F. Xie, D. Qu, Y. Zou, Y. Huang, H. Li, C. Zhao, P. Tan, M. Yu, Y. Fan, H. Zhang, Z.L. Wang, Z. Li, *Adv. Funct. Mater.* 29 (2019) 1807560.
- [21] Q. Shi, C. Lee, *Adv. Sci.* 6 (2019) 1900617.
- [22] J. Wang, H. Wang, T. He, B. He, N.V. Thakor, C. Lee, *Adv. Sci.* 6 (2019) 1900149.
- [23] Q. Shi, Z. Zhang, T. Chen, C. Lee, *Adv. Sci.* 62 (2019) 355–366.
- [24] W. Liu, Z. Wang, G. Wang, G. Liu, J. Chen, X. Pu, Y. Xi, X. Wang, H. Guo, C. Hu, Z. L. Wang, *Nat. Commun.* 10 (2019) 1426.
- [25] Y. Li, G. Cheng, Z.-H. Lin, J. Yang, L. Lin, Z.L. Wang, *Nano Energy* 11 (2015) 323–332.
- [26] M. Han, X.S. Zhang, X. Sun, B. Meng, W. Liu, H. Zhang, *Sci. Rep.* 4 (2014) 4811.
- [27] B. Zhang, J. Chen, L. Jin, W. Deng, L. Zhang, H. Zhang, M. Zhu, W. Yang, Z. L. Wang, *ACS Nano* 10 (2016) 6241–6247.
- [28] Y. Xi, H. Guo, Y. Zi, X. Li, J. Wang, J. Deng, S. Li, C. Hu, X. Cao, Z.L. Wang, *Adv. Energy Mater.* 7 (2017) 1602397.
- [29] H. Zhang, Y. Yang, Y. Su, J. Chen, K. Adams, S. Lee, C. Hu, Z.L. Wang, *Adv. Funct. Mater.* 24 (2014) 1401–1407.
- [30] H. Zhang, Y. Yang, Y. Su, J. Chen, C. Hu, Z. Wu, Y. Liu, C. Ping Wong, Y. Bando, Z. L. Wang, *Nano Energy* 2 (2013) 693–701.
- [31] S. Cui, Y. Zheng, T. Zhang, D. Wang, F. Zhou, W. Liu, *Nano Energy* 49 (2018) 31–39.
- [32] A.S.M.I. Uddin, G.-S. Chung, *Sens. Actuators, B* 231 (2016) 601–608.
- [33] Z. Wang, S. Yang, S. Miao, Q. Shi, T. He, C. Lee, *Nanomaterials* 9 (2019) 690.
- [34] L. Lin, Y. Xie, S. Wang, W. Wu, S. Niu, X. Wen, Z.L. Wang, *ACS Nano* 7 (2013) 8266–8274.
- [35] Y. Yang, H. Zhang, J. Chen, Q. Jing, Y.S. Zhou, X. Wen, Z.L. Wang, *ACS Nano* 7 (2013) 7342–7351.
- [36] D. Liu, X. Yin, H. Guo, L. Zhou, X. Li, C. Zhang, J. Wang, Z.L. Wang, *Sci. Adv.* 5 (2019), eaav6437.
- [37] X. Pu, H. Guo, J. Chen, X. Wang, Y. Xi, C. Hu, Z.L. Wang, *Sci. Adv.* 3 (2017), e1700694.
- [38] J. Peng, S.D. Kang, G.J. Snyder, *Sci. Adv.* 3 (2017), eaap8576.
- [39] Q. Zheng, Y. Zou, Y. Zhang, Z. Liu, B. Shi, X. Wang, Y. Jin, H. Ouyang, Z. Li, Z. L. Wang, *Sci. Adv.* 2 (2016), e1501478.
- [40] X. Pu, M. Liu, X. Chen, J. Sun, C. Du, Y. Zhang, J. Zhai, W. Hu, Z.L. Wang, *Sci. Adv.* 3 (2017), e1700015.
- [41] F. Yi, X. Wang, S. Niu, S. Li, Y. Yin, K. Dai, G. Zhang, L. Lin, Z. Wen, H. Guo, *Sci. Adv.* 2 (2016), e1501624.
- [42] Z. Wen, M.-H. Yeh, H. Guo, J. Wang, Y. Zi, W. Xu, J. Deng, L. Zhu, X. Wang, C. Hu, *Sci. Adv.* 2 (2016), e1600097.
- [43] J.W. Lee, H.J. Cho, J. Chun, K.N. Kim, S. Kim, C.W. Ahn, I.W. Kim, J.-Y. Kim, S.-W. Kim, C. Yang, *Sci. Adv.* 3 (2017), e1602902.
- [44] H. Guo, X. Pu, J. Chen, Y. Meng, M.-H. Yeh, G. Liu, Q. Tang, B. Chen, D. Liu, S. Qi, *Sci. Robot.* 3 (2018) eaat2516.
- [45] Y. Bai, L. Xu, C. He, L. Zhu, X. Yang, T. Jiang, J. Nie, W. Zhong, Z.L. Wang, *Nano Energy* 66 (2019) 104117.
- [46] T. He, Q. Shi, H. Wang, F. Wen, T. Chen, J. Ouyang, C. Lee, *Nano Energy* 57 (2019) 338–352.
- [47] T. He, Z. Sun, Q. Shi, M. Zhu, D.V. Anaya, M. Xu, T. Chen, M.R. Yuce, A.V.-Y. Thean, C. Lee, *Nano Energy* 58 (2019) 641–651.
- [48] T. Chen, Q. Shi, M. Zhu, T. He, Z. Yang, H. Liu, L. Sun, L. Yang, C. Lee, *Nano Energy* 60 (2019) 440–448.
- [49] Z. Qian, R. Li, J. Guo, Z. Wang, X. Li, C. Li, N. Zhao, J. Xu, *Nano Energy* 64 (2019) 103900.
- [50] F. Wen, H. Wang, T. He, Q. Shi, Z. Sun, M. Zhu, Z. Zhang, Z. Cao, Y. Dai, T. Zhang, *Nano Energy* (2019) 104266.
- [51] C. Jiang, X. Li, Y. Yao, L. Lan, Y. Shao, F. Zhao, Y. Ying, J. Ping, *Nano Energy* 66 (2019) 104121.
- [52] M. Ma, Z. Zhang, Z. Zhao, Q. Liao, Z. Kang, F. Gao, X. Zhao, Y. Zhang, *Nano Energy* 66 (2019) 104105.
- [53] Y. Jie, H. Zhu, X. Cao, Y. Zhang, N. Wang, L. Zhang, Z.L. Wang, *ACS Nano* 10 (2016) 10366–10372.
- [54] Y. Zi, H. Guo, J. Wang, Z. Wen, S. Li, C. Hu, Z.L. Wang, *Nano Energy* 31 (2017) 302–310.
- [55] Y. Zi, J. Wang, S. Wang, S. Li, Z. Wen, H. Guo, Z.L. Wang, *Nat. Commun.* 7 (2016) 10987.
- [56] G. Cheng, Z.-H. Lin, L. Lin, Z.-I. Du, Z.L. Wang, *ACS Nano* 7 (2013) 7383–7391.



Shuting Liu received her B.Eng. degree from the School of Electronic and Information Engineering, Tiangong University, Tianjin, China, in 2015. She is now a Ph. D. candidate in the College of Information Science and Electronic Engineering, Zhejiang University. Her research interests include resistive random access memory device, triboelectric nanogenerator, energy harvesters, and self-powered sensors.



Associate Prof. Hao Wang received his B.Eng. degree in School of Optoelectronic Information from University of Electronic Science and Technology of China in 2010, and Ph.D. degree from the National University of Singapore in 2016. He is currently a Research Associate of SIAT (Shenzhen Institutes of Advanced Technology), China. His research interests are focused on nanoneedle devices for transdermal drug delivery, flexible and wearable electronics, energy harvesting and electrical neural stimulations.



Prof. Shurong Dong received his Ph.D. degree in College of Information Science and Electronic Engineering from Zhejiang University in 2003. His current research interests include flexible electronics, mechanical energy harvesting through triboelectric nanogenerators (TENG), electronic discharge Protection on Chip (ESD), thin films acoustic bulk wave and surface acoustic wave resonator technology (FBAR, Saw). He is a Member and Vice-president of IEEE EDSHZ Chapter, a Member of the China Vacuum Academy, and a Member and Chair of the Zhejiang Vacuum Academy.



Tianyiyi He received her B.Eng. degree from the School of Microelectronics and Solid-state Electronics at the University of Electronic Science and Technology of China (UESTC), Chengdu, China, in 2016. She is now a Ph.D. candidate in the Department of Electrical and Computer Engineering, National University of Singapore. Her research interests include energy harvesters, triboelectric nanogenerator, thermoelectric energy harvester, and wearable sensors.



Chengkuo Lee received his Ph.D. degree in Precision Engineering from The University of Tokyo in 1996. Currently, he is the director of Center for Intelligent Sensors and MEMS at National University of Singapore, Singapore. He was a Senior Member of IEEE. He has contributed to more than 300 peer-reviewed international journal articles. His ORCID is 0000-0002-8886-3649.